*Korean J. Chem. Eng.*, 37(12), 2124-2135 (2020)
DOI: 10.1007/s11814-020-0645-8

pISSN: 0256-1115
eISSN: 1975-7220

# A multiscale study on the effects of dynamic capillary pressure in two-phase flow in porous media

**Jassem Abbasi*,**, Mojtaba Ghaedi*,***,†, and Masoud Riazi***

*Department of Petroleum Engineering, School of Chemical and Petroleum Engineering, Shiraz University, Shiraz, Iran
**Zodan Solutions Ltd., London, United Kingdom
***Reservoir Modeling and Simulation Centre, School of Chemical and Petroleum Engineering, Shiraz University, Shiraz, Iran
(*Received 17 May 2020 • Revised 18 July 2020 • Accepted 19 July 2020*)

**Abstract**−Capillary pressure is usually considered as a function of the rock and fluid properties, and saturation. However, recent studies have shown that capillary forces also are a function of the rate of change of saturation. Moreover, although it was observed that dynamic forces are highly scale dependent, the role of these effects in large-scale flow practices is still unclear. In this study, using an innovative numerical simulation approach, the impact of the mentioned parameters was studied in a highly heterogeneous oil reservoir that is under waterflooding process. It is observed that the role of dynamic capillary pressure, using routinely measured dynamic capillary coefficient values, is not important in large-scale problems. However, it would be important in the higher capillary coefficient values that are several orders of magnitude larger than the values reported in previous experimental studies. Furthermore, the role of rock heterogeneity is discussed and it is shown that neglecting the dynamic capillary effects in heterogeneous media may lead to misleading results in the prediction of the injection front behavior in the reservoir. The dynamic capillary effects, by lowering the imbibition capillary pressure in the front, leads to more frontal movement of the injection fluid. Also, it is shown that the dynamic effects are more sensible at points close to the injection wells in homogenous reservoirs, but, in the heterogenous models it is more dependent on rock properties than the distance from the injection wells.

Keywords: Dynamic Capillary Pressure, Dynamic Capillary Coefficient, Capillary Number, Waterflooding

## INTRODUCTION

The multiphase and unsaturated flow in porous media is highly under the control of the capillarity effects [1]. Capillary pressure is a measure of the differences between the pressures of two phases in the interface of fluids. The results of different studies show that simply the capillary pressure can be dependent on the surface tension between the fluids, the pore size distribution of the porous media, the wettability of the rock, and also the temperature [2,3]. This relationship can be easily stated as the Young-Laplace equation as below [4]:

$$P_c = \frac{2\sigma\cos\theta}{r_c} \tag{1}$$

where $\sigma$ is the interfacial tension, $\theta$ is the contact angle and $r_c$ is the effective radius of the porous media in the interface of the fluids. As a general and practical rule, the capillary pressure is considered to be a function of the saturation of fluids in porous media, $f(S_w)$, named as static capillary pressure [5]. Currently, this assumption is being used in all of the modeling practices of fluid flow in porous media using relations like Darcy's law [6]. But, several experiments showed that the capillary effect is not only dependent on the saturation of fluids, but also on the rate of change of the wetting phase saturation, $(f(S_w, \partial S_w/\partial t))$, known as dynamic capillary pressure, $P_c^{dynamic}$ [7-13]. It is suggested that the main reason for the difference between dynamic and static capillary pressure is the difference between the magnitude of the contact angles in dynamic and static conditions [14]. For the drainage process, this effect leads to more capillary pressure, and for the imbibition process it results in lower capillary pressure values with respect to static capillary pressure values. Also, in the drainage process, this value is more significant in mixed wet systems, and in the imbibition process the value can be considerable in strongly wet systems. Barenblatt [12] and Hassanizadeh et al. [15] introduced models for accounting the non-equilibrium effects in fluid flow processes. The first assumes non-equilibrium behavior for both relative permeability and capillary pressure, while the last model just considers the dynamic capillary pressure effects. Based on the model introduced by Hassanizadeh et al. [15], the relation between static and dynamic capillary pressure may be defined as:

$$P_c^{dynamic} - P_c = \tau\frac{\partial S_w}{\partial t} \tag{2}$$

where, as defined above, $P_c$ is the capillary pressure at equilibrium conditions ($\partial S_w/\partial t=0$). Also, $\tau$ is the dynamic capillary coefficient (also capillary damping coefficient), which is a measure of the speed to reach an equilibrium condition. The measurement process of the $\tau$ can be found in previous studies [9,16,17]. However, although the definition of dynamic capillary pressure is clear, there is a large amount of uncertainty about the magnitude of the $\tau$ coefficient in different conditions. Stauffer [18] stated that the value of the capillary damping coefficient is not a function of saturation,

†To whom correspondence should be addressed.
E-mail: m.ghaedi@shirazu.ac.ir

while recent studies showed that it is absolutely a function of saturation [9,10]. The reason is that the time scales of layer flow are dependent on the thickness of the layer on the rock surface [19]. Also, Hanspal and Das [20] showed that it is a direct function of the system temperature. Joekar-Niasar and Hassanizadeh [21] showed that the dynamic capillary pressure effects can be highly influenced by the viscosity ratio of fluids. Amaziane et al. [22] investigated the effects of rock heterogeneities and stated that the higher the difference in permeability of block and fractures, the greater the capillary force will be non-equilibrium like. Abbasi et al. [23] showed that dynamic capillary effects may lead to dissimilarity of imbibition curves in different study scales. Several modeling and experimental studies have shown that the effect of the dynamic capillary pressure in lab-scale is considerable and should not be neglected. On the other hand, the importance of the dynamic effects in large scale systems is still completely ambiguous. Different studies show that $\tau$ values are highly dependent on the averaging length scale of wetting phase saturation [24]. Abidoye and Das [17] conducted general research on the effect of length scale on the $\tau$ value and observed that as domain scale changes, the magnitude of $\tau$ increases an order of magnitude. Recently, a few studies were conducted on the impact of dynamic capillary coefficients in large scale processes. Tian et al. [25] investigated the effects of dynamic capillary effects in a tight sandstone reservoir where the capillary effects are considerable. They concluded that considering the dynamic capillary effects can improve the validity of simulation results. Mohammad et al. [26] showed that considering dynamic capillary pressure is crucial in waterflooding processes. Also, Li et al. [27] by conducting some experimental analysis showed that the presence of fracture and heterogeneities results in more dynamic capillary coefficients. However, studies in large-scale processes like oil production, gas storage practices, and also fluid flow in subsurface aquifers are conducted by neglecting dynamic capillary effects, and it is not clear how the dynamic effects of capillary pressure influence the morphology of front displacement in the reservoir at large-scale scenarios. In this work, to cover the mentioned weaknesses, the effect of the dynamic capillary pressure in a field-scale two-phase flow process is investigated. For the first time, a multiscale simulation approach has been followed using a novel simulation algorithm recently developed by the authors [25]. Moreover, it is tried to discuss several vague points in the study of dynamic capillary effects related to the impact of heterogeneity. As far as the authors know, this subject has not been covered properly in previous studies and requires significant attention. Also, several recommendations for future studies are suggested. Providing solutions for the introduced challenges is essential for the implementation of dynamic capillary effects in field-scale studies in the future that will be interesting for researchers.

In the following, first, the mathematical approach of the study is introduced. Then, the characteristics of the used models are presented. Simulation results are discussed and the obtained results in several scales are compared. Finally, the paper is ended with some conclusions.

## METHOD OF STUDY

As was discussed earlier, the effect of the dynamic capillary pressure in large scale problems needs more careful study. In this work, an open-source prototyping code to mimic fluid flow in Darcy media, called Matlab Reservoir Simulation Toolbox (MRST), has been utilized [28]. Basically, similar to other available platforms, the dynamic capillary effect has not been included in this software. In this study, an implicit-iterative algorithm was applied to the incompressible two-phase flow solver of MRST to include the dynamic capillary effects that use a standard two-point flux-approximation (TPFA) method calculating pressure and saturations [29]. The implemented algorithm is introduced in the next section.

### 1. Modeling Approach

As previously discussed by Abbasi et al. [30], distributions of pressure and saturation are the key determiners in the two-phase flow in porous media. For this system, the mass conservation equation is the main governing equation for each phase and is written as:

$$\frac{\partial}{\partial t}(\phi S_p \rho_p) + \nabla \cdot (\rho_p \vec{v}_p) = \rho_p q_p \tag{3}$$

where $\rho$ is the liquid density and $\varphi$ the porosity. v is volumetric velocity and q demonstrates injection/production of each phase. Also, p is the investigating phase and here is written for wetting (w) and nonwetting (n) phases and can be related to each other as:

$$\sum_{i}^{p=n,\,w} S_i = 1 \tag{4}$$

In the above equation, $S_i$ is the phase saturation. The flow of fluids in the porous system can be modeled by Darcy equation that by accepting its assumptions, it can be written as:

$$v_p = -\frac{k_{rp} K}{\mu_\alpha}(P_p - \rho_p g \nabla z) \tag{5}$$

where K is the permeability of the rock, $\nabla z$ is the height difference and g is the constant of gravitational acceleration. Moreover, P, $k_r$, and $\mu$ are the phase pressure, relative permeability, and viscosity, respectively. So, Eqs. (5) and (6) can be rewritten as:

$$\frac{\partial}{\partial t}(\phi S_p \rho_p) + \nabla \cdot \left(\frac{\rho_p k_{rp} K}{\mu_p}(\nabla P_p - \rho_p g \nabla z)\right) = \rho_p q_p \tag{6}$$

These equations are extremely conjugated and strongly complex to solve. This complexity is due the difference in primary variables ($P_n - P_w$) as the input for calculation of the phase saturations [31]. To solve the above nonlinearity, the system is defined in the form of one phase pressure and saturation:

$$\frac{\partial}{\partial t}(\phi S_w \rho_w) + \nabla \cdot \left(\frac{\rho_w k_{rw} K}{\mu_w}(\nabla P_n - \nabla P_c(S_w) - \rho_w g \nabla z)\right) = \rho_w q_w \tag{7}$$

$$\frac{\partial}{\partial t}(\phi(1 - S_w)\rho_n) + \nabla \cdot \left(\frac{\rho_n k_{rn} K}{\mu_n}(\nabla P_n - \rho_n g \nabla z)\right) = \rho_n q_n \tag{8}$$

For simplicity, it can be written:

$$P_n - P_w = P_c \tag{9}$$

This equation can be utilized as the complementary equation for reducing the order of the calculations. In the routine macroscale fluid flow in porous media calculations (Darcy's law), it is presumed that the $P_c$ is solely dependent on the phase saturations. Consider-

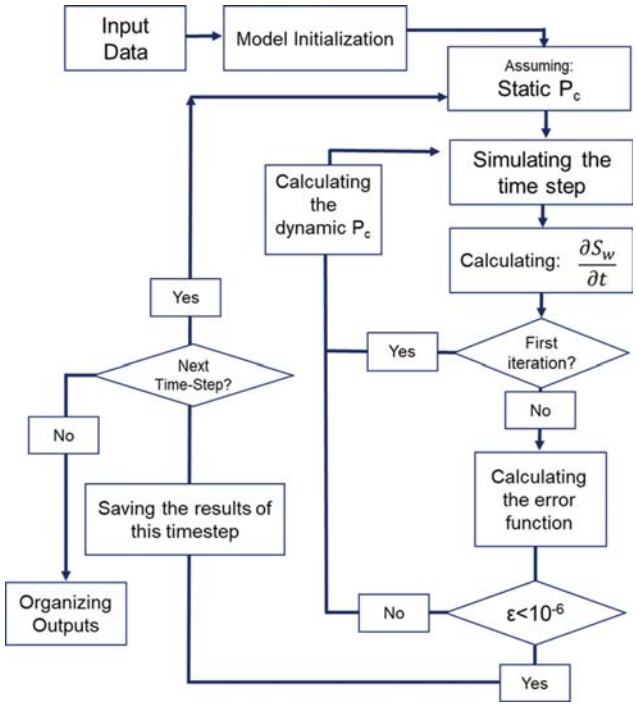


**Fig. 1. The algorithm defined for the implementation of dynamic capillary pressure.**

ing the importance of the dynamic phenomenon in $P_c$, Eq. (9) is modified as:

$$P_n - P_w = P_c - \tau\frac{\partial S_w}{\partial t} = P_c^{dynamic} \tag{10}$$

Using Eq. (10), Eq. (7) is rewritten as:

$$\frac{\partial}{\partial t}(\phi S_w \rho_w) + \nabla\cdot\left(\frac{\rho_w k_{rw} K}{\mu_w}(\nabla P_n - \nabla(P_c^{dynamic}) - \rho_w g \nabla z)\right) = \rho_w q_w \tag{11}$$

To find the solution of the above nonlinear equation in the required time and spatial space, numerical approaches such as finite difference methods are applied.

We used an iterative approach for finding the solution of the above equations; the related algorithm is shown in Fig. 1. From the algorithm, it is depicted that for each time-step, in the first iteration, the static $P_c$ is utilized to solve the pressure and phase saturation matrices. Using the obtained results, the degree of saturation changes vs. time ($dS_w/dt$) is determined for all of the cells as:

$$\frac{\partial S_w^N}{\partial t} = \frac{S_w^N - S_w^{N-1}}{\Delta t} \tag{12}$$

where N and Δt are the number of time-step and the length of the time-step, respectively. Then, using the following equation, the dynamic capillary pressure is calculated as:

$$P_c^{dynamic}(S_w^N) = P_c(S_w^N) - \tau\left(\frac{S_w^N - S_w^{N-1}}{\Delta t}\right) \tag{13}$$

The calculated $P_c^{dynamic}$ is employed for updating the pressure-saturation properties of cells in the current time-step and the next iteration. Recalculating the $dS_w/dt$ and $P_c^{dynamic}$ is followed until the convergence goal is reached. The stopping criterion for the iteration is when there is no considerable change in the wetting phase saturation. Based on this criterion, the error function ($\varepsilon$) can be calculated as:

$$\varepsilon = \frac{1}{C}\sum_{i=1}^{C}\left(\frac{S_w^{\nu,i} - S_w^{\nu-1,i}}{S_w^{\nu,i}}\right) \tag{14}$$

where C is the number of cells in the model, i is the number of the cell, and $\nu$ is the iteration number. If the obtained value of the error function reaches to less than the value of $10^{-7}$, the calculated results will be accepted and the calculations are passed to the next time-step. The above computations are carried out for all the defined time-steps. Non-equilibrium transport in porous media usually involves unsymmetrical matrices that require special consideration to ensure the robustness of the solution [32]. The size of the time-step, the grid dimensions, and the value of dynamic capillary coefficients have determining roles on the robustness of the simulation and the number of iterations required to reach the convergence.

It should be highlighted that the dynamic effects can influence both capillary pressure and relative permeability curves. In most of the previous studies [8,9,33], only the dynamic behavior of capillary pressure was discussed and influenced. Moreover, in this study the injection rates were low and flow was highly capillary dominated in most regions. So, the non-equilibrium characteristics of relative permeabilities are negligible. As a result, in this study, the dynamic capillary effects are solely used and the relative permeabilities are assumed to only be dependent on the phase saturations. The authors believe that these assumptions lead to interpretation simplicity and do not reduce the exactness and validity of the obtained results.

Because of the considerable rock heterogeneities, at first, we observed some convergence problems. To solve this problem, the time-steps were reduced and also the maximum iteration numbers were increased.

## 2. Model Description

Regarding the importance of considering a model with large heterogeneity, the static model of the 10th SPE comparative solution

**Table 1. A summary of the large-scale model**

| Property | Value | Property | Value |
|---|---|---|---|
| Cell number | 60×220×5 | Injection well number | 3 |
| Cell size (m) | 6×3×0.6 | Production well number | 8 |
| Average porosity (-) | 0.17 | Injection rate (STB/day) | 10 |
| Average permeability (md) | 355.4 | Production bottom-hole pressure (psia) | 4,000 |
| Initial oil saturation (-) | 1.0 | Total pore volume injected (-) | 0.22 |

project was used in this work. The SPE Comparative Solution Projects are generally used for an independent comparison of numerical methods. The SPE 10 model was introduced to examine different grid upscaling methods. Blunt et al. [34] compared the results of different simulators and introduced the best single-phase upscaling method. Originally, the fine model consists of 60×220×85 cells (1122000 cells). The cell sizes of the model are 6×30.6 (m) that are relatively fine. To ignore the unnecessary complexities, a sector that considers only five vertical layers (6 to 10) and one-half of the model (left side) were extracted from the original model for simulation of

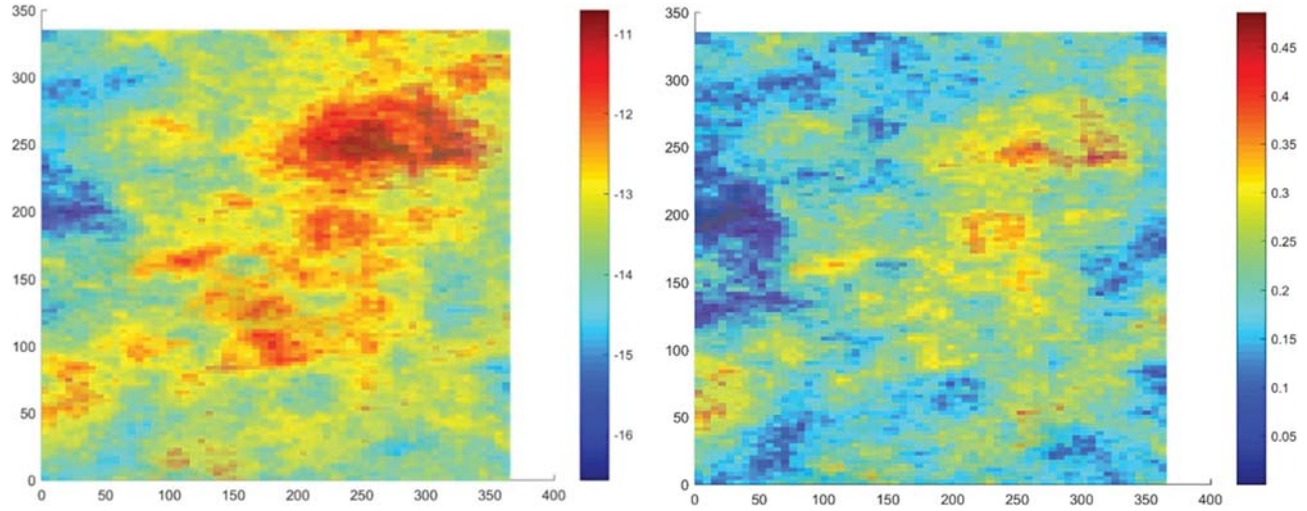


**Fig. 2. The areal log permeability map (left) and porosity map (right) of the considered sector of the SPE 10 Model.**

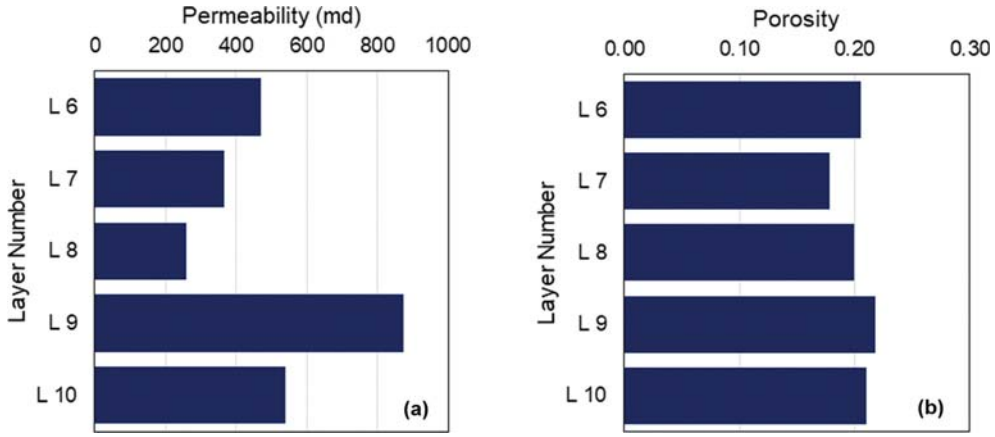


**Fig. 3. Average reservoir properties for different layers: (a) Permeability, (b) Porosity.**

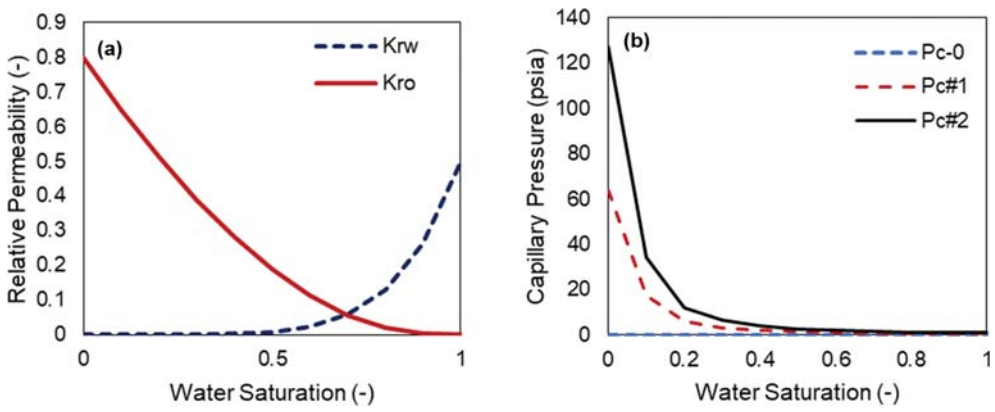


**Fig. 4. (a) The oil and water relative permeability curves, (b) Different scenarios of capillary pressure curves.**

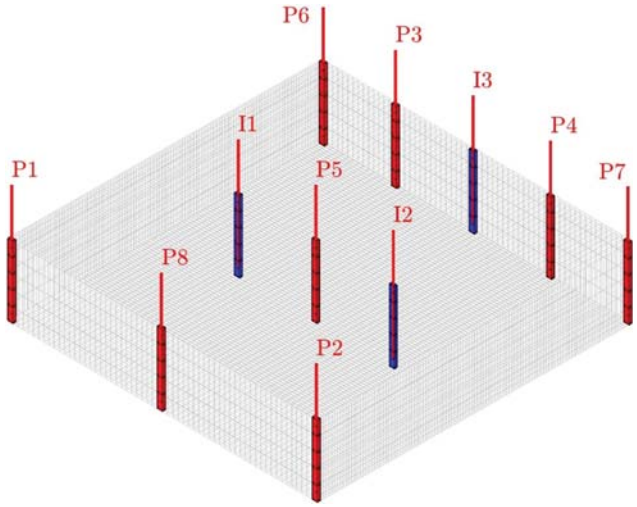


**Fig. 5. The injection (blue) and production (red) wells pattern.**

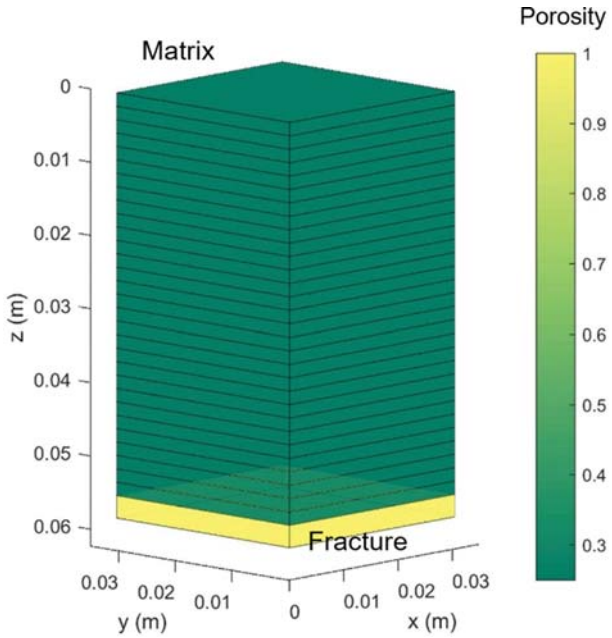


**Fig. 6. The geometrical model for fracture and matrix.**

the impacts of dynamic capillary effects in field-scale. Table 1 shows a summary of the properties of this model. Also, Fig. 2 shows the permeability and porosity map of the extracted model. As can be seen from the figure, the model is highly heterogeneous in the lateral direction. Also, the average permeability and porosity of each reservoir layer are shown in Fig. 3. It is also clear that the heterogeneity in the vertical direction is significant as well. The wettability of reservoir rock was set to be water wet. The related relative permeability curves are shown in Fig. 4(a). Also, the defined relative capillary pressure curves are presented in Fig. 4(b). As this figure shows, to understand the influence of capillary force in the considered scenarios, different capillary curves were assumed.

The waterflooding process is carried out using eight production and three injection wells. The production/injection pattern is shown in Fig. 5. As shown, the wells are not uniformly distributed in the reservoir. Also, all the wells are completed in all of the layers. The injection rate was 10 STB/day and the production wells were produced at the constant bottom-hole pressure of 4,000 psia.

Also, to compare the extent of dynamic capillary effects at different scales, a core scale imbibition simulation test was conducted. The geometrical schematic of the model is shown in Fig. 6. The model consisted of a matrix (upper) and a fracture (lower) with high pore volume (to have constant saturations in fracture medium). The fracture is filled with the water and the matrix is saturated with oil. As Table 2 shows, the areal cross-section of the model was 9 $cm^2$ and the height was 6 cm (with pore volume approximately similar to a routine core plug). Also, the matrix porosity and permeability were 0.25 and 355 md, respectively. The matrix relative permeability of phases was the same as the field model curves (Fig. 4(a)). Also, the Pc#2 curve (Fig. 4(b)) was used as the capillary pressure of the matrix. The capillary effects in fracture were negligible and the relative permeability curves were linear.

## RESULTS AND DISCUSSION

After initialization of the simulation models, different simulation scenarios in both field and core scale were conducted in the MRST simulator (provided in the following sections). It should be indicated that the flow process in these scenarios is highly capillary dominant due to the low injection rates.

In the following, before entering the discussion about the impact of dynamic capillary effects, at first, the behavior of the reservoir under waterflooding (by the assumption of static capillarity) is discussed.

### 1. The Impact of Capillary Pressure

As highlighted previously, studying the effects of dynamic capillary forces without a clear understanding of the effect of static capillary pressure is not reasonable. The relative importance of capillary effects in fluid flow in porous media is highly dependent on the pore structure of the rock. In large scale continua, with increasing the complexity, these effects are more substantial. Moreover, the presence of low capillary number values is important. The capil-

**Table 2. A summary of the core scale model**

| Property | Value | Property | Value |
|---|---|---|---|
| Cell number (matrix) | 1×1×30 | Fracture pore volume multiplier | 100 |
| Matrix cell size (cm) | 3×3×0.2 | Fracture cell size (cm) | 3×3×0.2 |
| Average matrix porosity | 0.25 | Average fracture porosity | 1 |
| Average matrix permeability (md) | 355 | Average fracture permeability (d) | 100 |

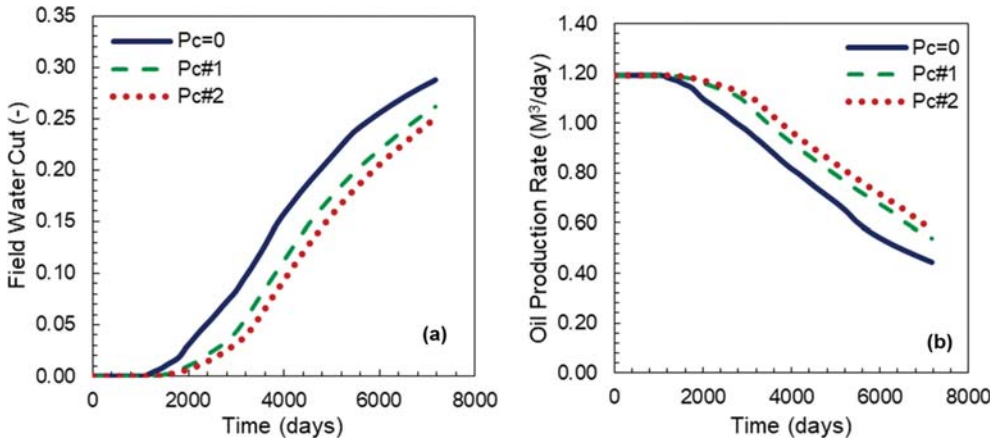


**Fig. 7. The impact of capillary pressure on the fluid flow, (a) field water-cut, (b) total oil production rate.**

lary number is a quantitative expression of the ratio of the buoyant (viscous) force to gradients in the capillary pressure. In this section, three different scenarios with different capillary pressure curves were considered. The capillary pressure curves are shown in Fig. 4(b). The field water-cut in different scenarios is presented in Fig. 7(a). The results show that by increasing the capillary pressure magnitude, the field water-cut is decreased. In this case, the production water cut after water breakthrough decreased by around five percent under the effects of capillary phenomena.

To understand the obtained results, it should be noted that the understudy continuum is highly heterogeneous, both horizontally and vertically (Fig. 2 and Fig. 3). The significant vertical heterogeneity of the porous media in stratified reservoirs usually leads to a fast breakthrough of the injection front in the high permeable layers. Increasing the magnitude of the capillary pressure affects the volumetric flux of the fluids in different layers. Since the viscous forces in low permeable layers are less, the influence of capillary forces is more significant than the high permeable layers. This leads to increasing the share of low permeable layers in the transmission of the fluids and, consequently, decreasing flux rate in a high permeable layer that eventually results in delaying the breakthrough of the injection front in production wells. Similar results are also observed in previous studies [35,36]. It is theorized that the impact of the rock heterogeneity on macroscopic flow is directly related to the continuum scale capillary number [37]. In the following sections, by including the dynamic capillary coefficient, the dynamic behavior of the considered field is investigated.

**Table 3. The considered scenarios of the dynamic capillary coefficient**

| Scenario | Capillary pressure curve number | Dynamic coefficient (Pa·s) |
|---|---|---|
| Pc#0Tau0 | 0 | 0 |
| Pc#2Tau0 | 2 | 0 |
| Pc#2Tau1e11 | 2 | $1\times10^{11}$ |
| Pc#2Tau2e11 | 2 | $2\times10^{11}$ |
| Pc#2Tau3e11 | 2 | $3\times10^{11}$ |
| Pc#2Tau4e11 | 2 | $4\times10^{11}$ |

## 2. Impact of Dynamic Capillary Effects

In this section, the effects of considering the dynamic capillary effects in various waterflooding scenarios are discussed. As previously stated, in this study the dynamic capillary coefficients are assumed constant and are not dependent on parameters like tempera-

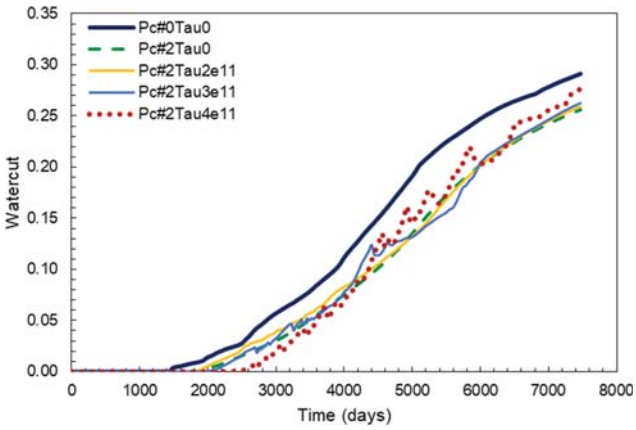


**Fig. 8. Water cut of the field versus time during waterflooding.**

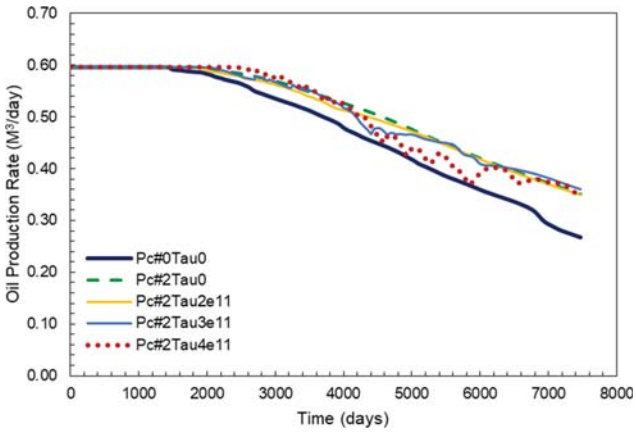


**Fig. 9. Oil production rate of the field versus time during waterflooding.**

ture and saturation. In this section, different scenarios with different dynamic capillary coefficient values are considered with details shown in Table 3. The considered capillary coefficient values are in the range of $1\times10^{11}$ to $4\times10^{11}$ Pa·s, which are several orders of magnitude larger than the values measured in the previous studies [8]. The values used for $\tau$ were obtained by several sensitivity analyses performed earlier. We tested several geological models with different reservoir/well configurations. The used range of $\tau$, $10^{11}$ Pa·s, is the range that the dynamic capillary pressure is observable and also reliable. The much lower values make the effects of dynamic capillary pressure negligible (same as the scenario with static capillary pressure); the much higher values practically make the last term of Eq. (13) very large, and the capillary pressure will be zero that do not have any physical meanings (same as the scenario without any capillary pressure). Therefore, a suitable range for the value of the dynamic capillary coefficient is the values already used.

Fig. 8 shows the total field water cut versus time for different simulation scenarios (Table 3). The figure shows that in the scenario with dynamic capillary coefficient $\tau=1\times10^{11}$ Pa·s, the field water cut was not considerably influenced by the dynamic capillary effects. Moreover, in lower dynamic capillary coefficients, the reservoir behavior is not influenced by the dynamic capillary effects as well. By considering the value of $4\times10^{11}$ for the dynamic capillary coefficient, the water cut curve deviated from the static conditions. As Fig. 8 shows, in this scenario the breakthrough time is delayed in comparison with the static capillary case. After a short time, the water cut excelled from the scenario with the static capillary coefficient. As the figure shows, the water cut in this scenario did not

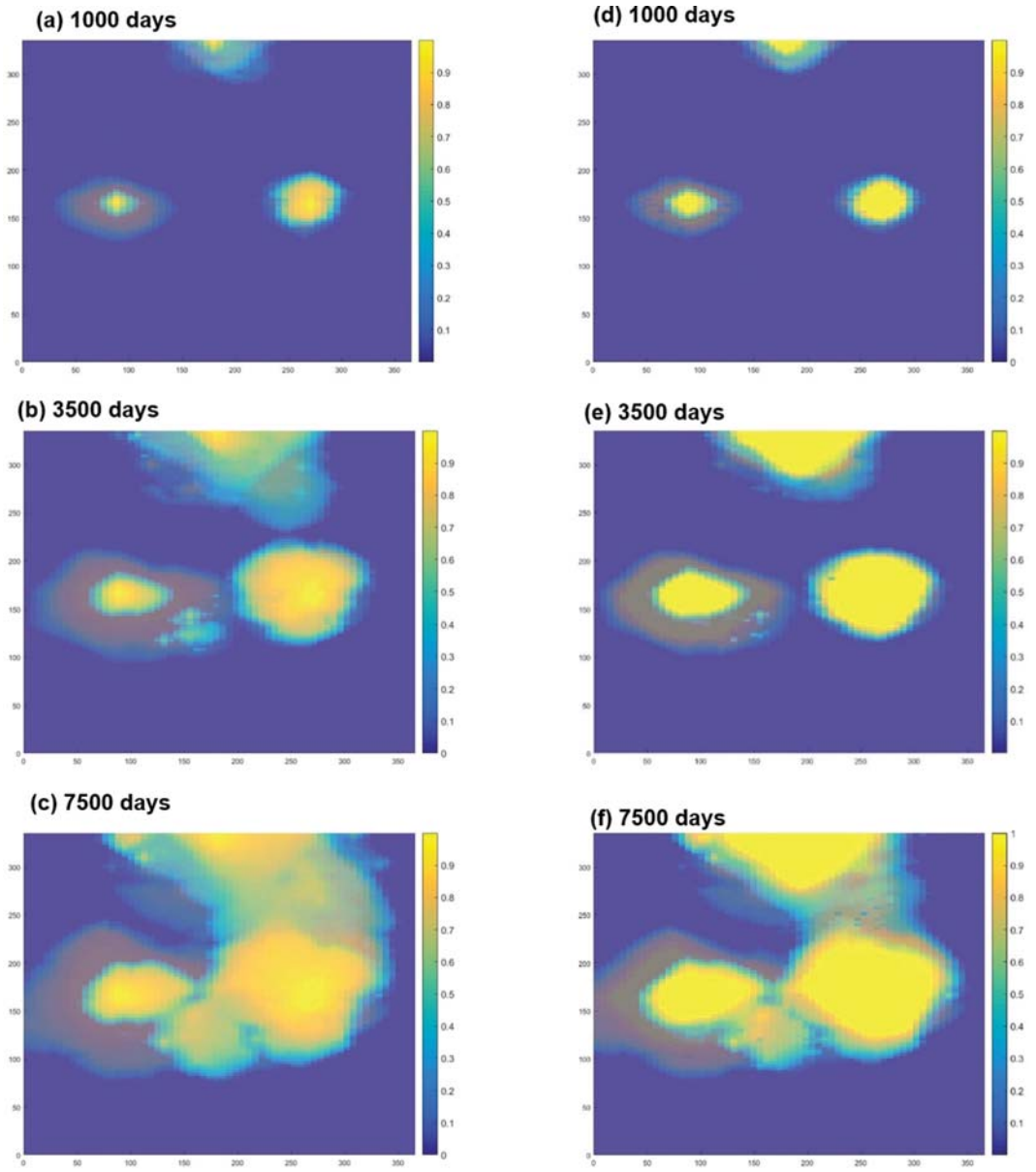


**Fig. 10. The map of water saturation in different simulation times (after 1,000, 3,500, and 7,500 days) for scenarios with static ((a), (b), (c)) and dynamic capillary pressure with $\tau=4\times10^{11}$ Pa·s ((d), (e), (f)).**

experience a smooth trend. These noises can be due to the heterogeneity of the reservoir rock. In this condition, the injection front faces with different propagating velocities at the interface of the front. Fig. 10 shows the water saturation map during water injection for scenarios with (Pc#2Tau4e11) and without (Pc#2Tau0) considering the dynamic capillary coefficient. It can be seen that in both scenarios the general trend of front movement is approximately similar. But, the propagation of injected water in the case with the dynamic capillary coefficient is slower than the other case. Another important difference between the water propagation in two scenarios is that in the case with the dynamic capillary coefficient the injection front moved more frontally [38]. It means that in the case with dynamic capillary pressure, the water saturation in the front experienced a sharper decrease from the injection side to the production side in comparison with the case with static capillary pressure. The water saturation in the water invaded zone is almost 1 in Pc#2Tau4e11 scenario, but in the scenario with static capillary pressure, it is lower (almost 0.8). In Fig. 8, by comparing the water cut curves of the two scenarios with and without applying dynamic capillary coefficient (Table 3), it can be claimed that in the scenario of Pc#2Tau4e11 the production water cut stayed lower than the base case (Pc#2Tau0) at initial times of simulation (for around 4,000 days) and then went higher. This behavior can be interpreted by attention to the effect of the dynamic capillary coefficient in improving the frontal behavior of the injection front. Also, Fig. 9 shows the oil production rate of the field versus the simulation time. As this figure shows, by increasing the dynamic coefficient the oil production rate is decreased with respect to the case with the static capillary curve.

The obtained results also can be confirmed by comparing the trends of the time derivative of saturation in Fig. 11. As the figure shows, the values of the time derivative of saturation have a grad-

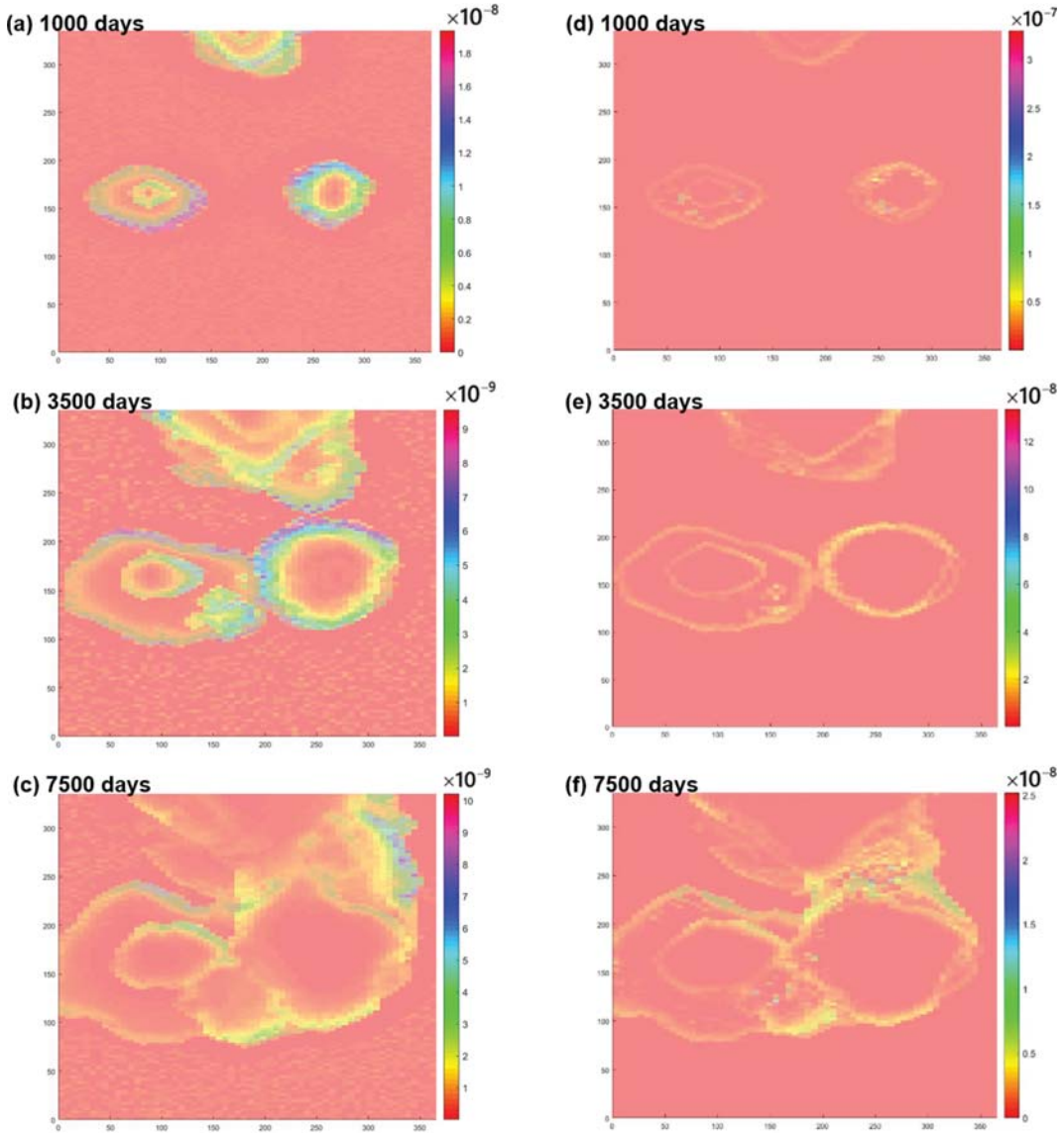


**Fig. 11. A map of the time derivative of water saturation ($\partial S_w/\partial t$) in different simulation times (after 1,000, 3,500, and 7,500 days) for scenarios with static capillary pressure ((a), (b), (c)) and dynamic capillary pressure with $\tau=4\times10^{11}$ Pa·s ((d), (e), (f)).**

ual distribution in the scenario with static capillary pressure, while in the case with dynamic capillary pressure, the changes of water saturation are only on a thin layer at the injection front. However, in the last case, the value of $\partial S_w/\partial t$ is around one order of magnitude larger than the values in the case with the assumption of static capillary pressure. Generally, from this part of the study, it can be concluded that in the considered field case, the effect of dynamic characteristics of capillary pressure is not significant when the dynamic capillary coefficient is lower than $1\times10^{10}$ Pa·s. But in the cases with a higher dynamic capillary coefficient, the reservoir behavior is affected. Of course, this critical value of dynamic capillary coefficient may be different in other field cases with different rock and injection/production characterizations. As stated previously, the measured values for the dynamic capillary coefficient in previous studies (in core scale) are in the range of $10^5$ to $10^8$ Pa·s, which is much lower than the effective values found in this study. Naturally, there are many differences between the flow processes in porous media in core scale and in field-scale that should be investigated to reach to a good view on the possible effects of the dynamic capillary pressure in field-scale practice. This means that considering the dynamic capillary coefficient may result in considerably different outputs. Note that in an imbibition process (like a water injection process), the effective capillary pressure is lower than static capillary pressure. A discussion about this topic is provided in the next sections of this study.

## 3. Multiscale Study

As previously indicated, multiphase flow in porous media is highly under the impact of geological heterogeneity of the porous domain. The flow in heterogeneous porous media generally has multiscale solutions [39]. This section attempts to provide some discussion about the impact of geological heterogeneity on the extent of the dynamic capillary pressure in different areal locations by comparing waterflooding process in two different homogeneous and heterogeneous models. Fig. 12 shows the value of time derivative of water saturation, $\partial S_w/\partial t$ (at the injection front) for two heterogeneous and homogenous models. These results can be compared with the distribution of rock porosity and permeability in a heterogeneous model that is shown in Fig. 2. Also, the average values of rock permeability and porosity of the heterogeneous model were calculated and used in the homogeneous model. As Fig. 12(a) shows, the time derivative of water saturation has a power (inverse) trend versus distance from the injection source in the homogeneous model (with $R^2$=0.2602). But, as Fig. 12(b) shows, the value $\partial S_w/\partial t$ does not follow any particular trend in the heterogeneous reservoir ($R^2$=0.0076 that is so small). In fact, in the heterogeneous case, the $\partial S_w/\partial t$ is a function of distance and also the reservoir properties. This is because the value of $\partial S_w/\partial t$ in high permeability zones is greater than the values in low permeability zones. Also, from Fig. 12 it can be concluded that the rate of change in water saturation experienced more values in the heterogeneous case in comparison to the homogeneous one. From this figure, it can be found that in homogeneous reservoirs the rate of change of saturation ($\partial S_w/\partial t$) and consequently the dynamic capillary effect is more prominent in regions close to the injection source. But in the heterogeneous reservoir, the prediction of the effects of dynamic capillary pressure versus areal location is complicated [27]. In these

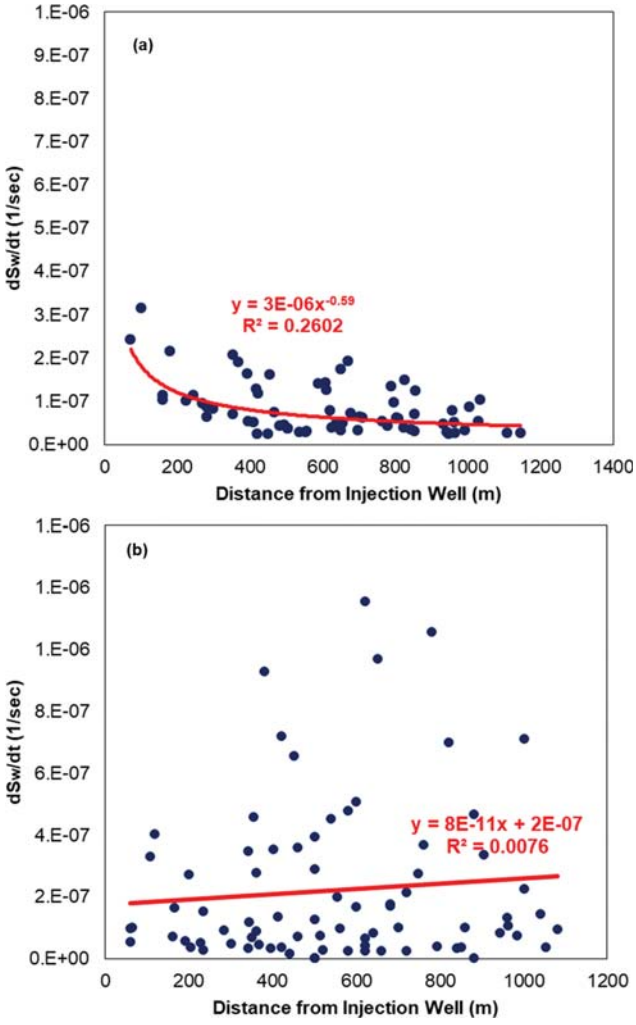


**Fig. 12. The derivative of water saturation at different distances from the injection well for (a) homogeneous domain (b) heterogeneous domain.**

kinds of reservoirs, the dynamic capillary effects in lateral and vertical directions are location-dependent (Fig. 12(b)). From this part, it can be concluded that the reservoir property and heterogeneity of the properties should be critically considered in the pore to the field-scale study of dynamic capillary effects. Moreover, it needs to be indicated that the distribution of $\partial S_w/\partial t$ in the reservoir can also be affected by the geometry of placement of the wells.

Fig. 13 shows the value of the time derivative of water saturation for each cell versus the rock properties of the cell for a specific time step. It can be seen that the value of $\partial S_w/\partial t$ (as expected) has a moderate functionality with the rock permeability and porosity. Also, it can be seen that the rate of change of saturation may be orders of magnitude different in various points of a heterogeneous reservoir. By seeing this behavior, deep studies can be suggested on the dependency of dynamic capillary pressure and dynamic capillary coefficient to the static and dynamic specifications of the flowing porous media, such as flow velocity, rock transmissibility/permeability.

On the other hand, during the investigation of dynamic capil-

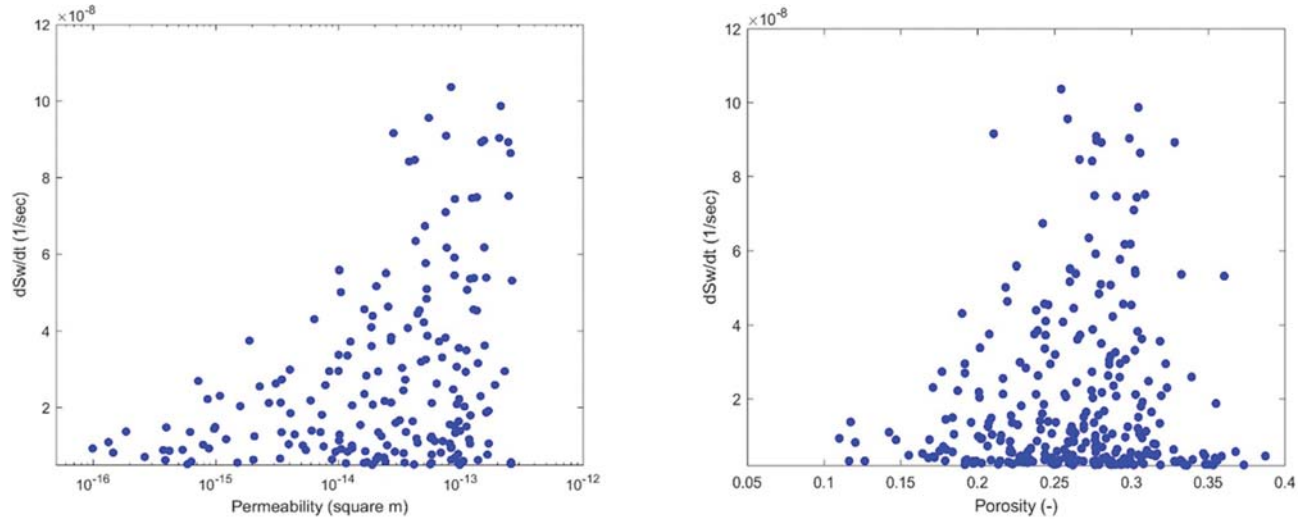


**Fig. 13. The time derivative of water saturation for each cell versus rock properties in a specific time step (a) Permeability (b) Porosity.**

lary effects, the differences between flow behaviors in different scales need to be considered. Since different parameters like temperature, the structure of the porous media, and fluid properties are effective on dynamic capillary pressure and these parameters usually significantly change through different scales, studying of the scale dependency of dynamic capillary force is complex and the obtained conclusions maybe highly case dependent [17]. So, the dynamic flow behavior of fluids in porous media may be highly different between small (core scale) and large-scale scenarios.

To reach to a general view, a core scale simulation test was conducted to compare the magnitude of $\partial S_w/\partial t$ in small and large scales. Fig. 6 shows the schematic of the simulated core. Fig. 14 shows the values of the time derivative of saturation for points with different distances from the matrix/fracture face. As expected, the maximum value of $\partial S_w/\partial t$ is greater in points close to the fracture face. Also, the magnitude of $\partial S_w/\partial t$ is around $10^{-3}$ $sec^{-1}$ at points close to the fracture and around $10^{-5}$ $sec^{-1}$ at points relatively far from the fracture face. Recent studies also revealed that in a core scale imbibition process, the time derivative of saturation is generally in the range of $10^{-6}$ to $10^{-3}$ $sec^{-1}$, in the imbibition front [30]. Of course, at the points far from the front, this range can be much lower (in the range of $10^{-8}$ $sec^{-1}$). However, this range may be much different in large-scale flow processes. As Fig. 11 shows, the time derivative of saturation is in the range of $10^{-8}$ $sec^{-1}$ in the case with dynamic capillary coefficient and $10^{-9}$ $sec^{-1}$ in the case with the static capillary coefficient. These values are much less than the values observed at the core scale. The main reason behind this difference is the difference between the cell sizes used in the field-scale numerical simulation. By comparing the sizes of cells in two models, it can be seen that the cell sizes increase around five orders of magnitude from the core model to field model. On the other hand, comparing the values of the time derivative of saturation shows that the value of $\partial S_w/\partial t$ in core scale is around four to six orders of magnitude larger than the field-scale values. This challenge is also present in experimental measurements. Several studies revealed that there are dependencies between the length scale of averaging the saturations and the value of the measured capillary dynamic coefficients and also dynamic capillary pressure [8]. Dahle et al. [40] stated that the dynamic capillary coefficient is a square function of the averaged length scale. Also, lower-order dependencies were suggested by Abidoye and Das [17]. It seems that the length scale dependency of dynamic capillary pressure is a critical challenge for measurement and characterization of dynamic capillary phenomena, especially in the case of upscaling of experimental results for use in field-scale studies. By the way, in addition to the differences between averaging length scales between core and field-scale scenarios, the flow velocity of fluids along the porous media may also be different in two investigating scales that may lead to different $\partial S_w/\partial t$ values. Considering the results obtained in previous studies, the magnitude of the dynamic capillary coefficient has an inverse functionality with the time derivative of water saturation [17]. Regarding the stated observations, it can be highlighted that the magnitude of the dynamic coefficient can be higher

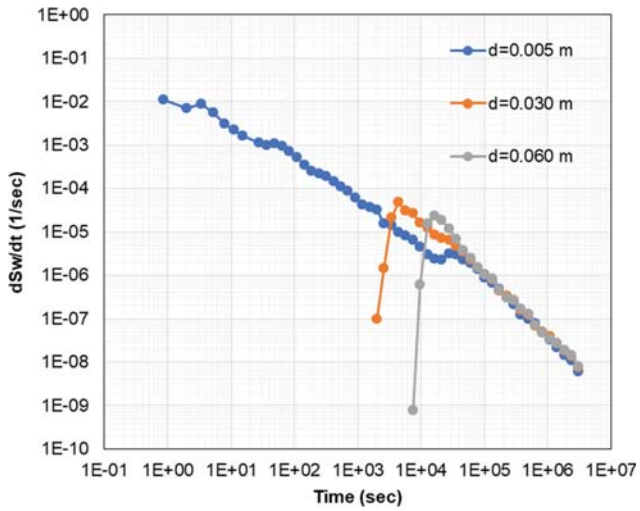


**Fig. 14. The time derivative of water saturation in the core scale imbibition process for different locations of the core (distance assumed from the fracture face).**

in field-scale processes due to differences in the flow velocity and also averaging domain of saturation changes ($\partial S_w/\partial t$). Furthermore, it is clear that the deviation of capillary pressure from static conditions is different in different locations of the reservoir and using a capillary curve measured at dynamic conditions cannot retrieve the real processes occurring in dynamic conditions.

Also, based on results by Hanspal and Das [20], the $\tau$ value increases by increasing the temperature. So, since the reservoir temperature is usually more than the core scale laboratory tests, the dynamic capillary coefficient is probably more important in actual fields than the ambient experimental measurements. Moreover, the $\tau$ value is more considerable in dense rocks where the porosity and permeability values are very low. So, it can be predicted that the magnitude of $\tau$ in field-scale processes is greater in comparison with the values obtained in core scale measurements. By the way, although the results obtained in this study show that dynamic capillary effects can be significant in field-scale studies, the used dynamic capillary coefficients are more than the routine values measured in the laboratory, due to differences between the averaging distances of the saturation. So, more investigation is recommended to measure or predict the magnitude of dynamic capillary coefficient in more realistic conditions, including high temperature and heterogeneous cases, that can be a better representative of field-scale scenarios. Finding general correlations is necessary for correctly applying dynamic capillary effects in these conditions. Also, to calibrate the developed correlations for each specified reservoir, a set of standard experimental/numerical approaches may need to be established.

## CONCLUSIONS

In this study, the significance of the dynamic capillary pressure effect in a two-phase flow scenario at field-scale was investigated. First, the effect of capillary pressure was investigated and the results showed that increasing capillary pressure leads to more frontal movement of injection front. The influence of dynamic capillary pressure on large scale models was studied next. With attention to the obtained results, it was observed that the breakthrough time was delayed by increasing the dynamic capillary pressure coefficient. Moreover, the results showed that increasing the dynamic capillary pressure coefficient causes the field water-cut to be lower at initial times of injection and then higher after a period of time than the scenario with the assumption of static capillary pressure. These impacts were observed when the dynamic capillary coefficient was larger than $10^{11}$ Pa·s. This value is much more than the values previously measured in laboratory-scale studies. Moreover, the magnitude of the $\partial S_w/\partial t$ in field and core scales was compared and their magnitudes were completely different. These differences are mostly because of the differences between the averaging length scale of the saturations that is a weakness of the current modeling approaches. It seems that defining the dynamic capillary pressure based on other parameters like the front velocity is more in agreement with the realistic phenomenon of dynamic capillary effects, and also it is more practical for upscaling of the experimental measurements. It needs to be concluded that direct usage of experimentally measured dynamic capillary coefficient values in field-scale studies is not viable and any comprehensive theory is still recommended on this issue. Finally, the results showed that increasing heterogeneities in the model makes the prediction of dynamic capillary effects at different locations of the field more complicated.

## ACKNOWLEDGEMENT

The authors would like to appreciate the Sintef co. for providing Matlab Reservoir Simulation Toolbox (MRST) and also Dr Knut-Andreas Lee for their worthy support during this project. Moreover, the financial and scientific support from EOR Research Centre at Shiraz University and also Reservoir Modeling and Simulation Centre (RMSC) is highly acknowledged.

## REFERENCES

1. M. K. Rahman, Z. Chen and S. S. Rahman, *J. Energy Resour. Technol.*, **125**, 169 (2003).
2. J. Bear, *Modeling phenomena of flow and transport in porous media*, Vol. 31, Springer, New York (2018).
3. J. Abbasi, M. Riazi, M. Ghaedi and A. Mirzaei-Paiaman, *J. Pet. Sci. Eng.*, **150**, 108 (2017).
4. R. F. John, *Principles of applied reservoir simulation*, Elsevier, Netherland (2001).
5. Z. Fan, D. Yang, D. Chai and X. Li, *J. Energy Resour. Technol.*, **141**, 2 (2018).
6. M. Zhang and L. F. Ayala, *J. Energy Resour. Technol.*, **142**, 4 (2019).
7. D. B. Das and S. M. Hassanizadeh, *Upscaling multiphase flow in porous media*, Springer, Berlin (2005).
8. S. Bottero, S. M. Hassanizadeh, P. J. Kleingeld and A. Bezuijen, *Experimental study of dynamic capillary pressure effect in two-phase flow in porous media*, In Proceedings of the XVI International Conference on Computational Methods in Water Resources (CMWR), Copenhagen, Denmark (2006).
9. D. B. Das and M. Mirzaei, *AIChE J.*, **58**, 3891 (2012).
10. M. Mirzaei and D. B. Das, *Chem. Eng. Sci.*, **62**, 1927 (2007).
11. R. Juanes, *Adv. Water Resour.*, **31**, 661 (2008).
12. G. I. Barenblatt, Izv. *Akad. Nauk SSSR, Mekh. Zhidk. Gaza*, **5**, 144 (1971).
13. Y. Shi and D. Yang, *J. Energy Resour. Technol.*, **139**, 062902 (2017).
14. S. Manthey, S. M. Hassanizadeh and R. Helmig, *Upscaling multiph. Flow porous media from pore to core beyond*, Springer, Berlin (2005).
15. S. M. Hassanizadeh, M. A. Celia and H. K. Dahle, *Vadose Zo. J.*, **1**, 38 (2002).
16. D. A. DiCarlo, M. Mirzaei and K. Jessen, *SPE J.*, **16**, 812 (2011).
17. L. K. Abidoye and D. B. Das, *Adv. Water Resour.*, **74**, 212 (2014).
18. F. Stauffer, IAHR symposium on scale effects in porous media, Thessaloniki, Greece, 29, 3-35 (1978).
19. M. J. Blunt, *Multiphase flow in permeable media*, Cambridge University Press, London (2017).
20. N. S. Hanspal and D. B. Das, *AIChE J.*, **58**, 1951 (2012).
21. V. Joekar-Niasar and S. M. Hassanizadeh, *Int. J. Multiph. Flow*, **37**, 198 (2011).
22. B. Amaziane, J. P. Milišić, M. Panfilov and L. Pankratov, *Phys. Rev.*

*E - Stat. Nonlinear, Soft Matter Phys.*, **31**, 9 (2012).
23. J. Abbasi, M. Ghaedi and M. Riazi, Saint Petersburg 2018: Innovations in Geosciences, Saint Petersburg (2018).
24. S. Bottero, S. M. Hassanizadeh and L. J. Pyrak-Nolte, AGU Fall Meeting Abstracts, Alberta (2009).
25. L. Tian, B. Feng, S. Zheng, D. Gu, X. Ren and D. Yang, *J. Energy Resour. Technol.*, **141**, 2 (2018)
26. R. S. Mohammad, M. Y. K. Tareen, A. Mengel, S. A. R. Shah and J. Iqbal, *J. Pet. Explor. Prod. Technol.*, **10**, 1891 (2020).
27. Y. Li, C. Liu, H. Li, S. Chen and S. Huang, *J. Hydrol.*, **584**, 124709 (2020).
28. K.-A. Lie, *Reservoir Simulation Toolbox (MRST)*, Cambridge University Press, 2019, London (2015).
29. H. M. Nilsen, K. A. Lie and O. Andersen, *Comput. Geosci.*, **20**, 49 (2016).
30. J. Abbasi, M. Ghaedi and M. Riazi, *J. Pet. Sci. Eng.*, **162**, 44 (2018).
31. K. A. Lie, S. Krogstad, I. S. Ligaarden, J. R. Natvig, H. M. Nilsen and B. Skaflestad, *Comput. Geosci.*, **16**, 297 (2012).
32. G. Gambolati and G. Pini, *Int. J. Numer. Methods Fluids*, **29**, 343 (1999).
33. D. B. Das, T. Thirakulchaya, L. Deka and N. S. Hanspal, *Environ. Process.*, **2**, 1 (2015).
34. M. A. Christie and M. J. Blunt, *SPE Reserv. Eval. Eng.*, **4**, 308 (2001).
35. Y. Debbabi, M. D. Jackson, G. J. Hampson and P. Salinas, *Transp. Porous Media*, **120**, 183 (2017).
36. Y. Debbabi, M. D. Jackson, G. J. Hampson, P. J. R. Fitch and P. Salinas, *Transp. Porous Media*, **117**, 281 (2017).
37. I. Chatzis and N. R. Morrow, *Soc. Pet. Eng. J.*, **24**, 555 (1984).
38. Y. Li, H. Li, S. Chen, Y. Lu, X. Li, H. Luo, C. Liu and X. Cui, Int. Pet. Technol. Conf., IPTC 2019, Beijing (2019).
39. T. Y. Hou, *Int. J. Numer. Methods Fluids*, **47**, 707 (2005).
40. H. K. Dahle, M. A. Celia and S. M. Hassanizadeh, *Upscaling multiph. Flow porous media from pore to core beyond*, Springer, Berlin, Germany (2005).